Radiation Physics and Chemistry 80 (2011) 561–566

Contents lists available at ScienceDirect

Radiation Physics and Chemistry

journal homepage: www.elsevier.com/locate/radphyschem

Non-destructive image analysis of soil surface porosity and bulk density dynamics

L.F. Pires [a,*], F.A.M. Cássaro [a], O.O.S. Bacchi [b], K. Reichardt [b]

[a] Laboratory of Soil Physics and Environmental Sciences, State University of Ponta Grossa, UEPG, C.E.P. 84.030-900, Ponta Grossa, PR, Brazil
[b] Laboratory of Soil Physics, Center for Nuclear Energy in Agriculture, USP/CENA, C.P. 96, C.E.P. 13.400-970, Piracicaba, SP, Brazil

ARTICLE INFO

Article history:
Received 26 August 2009
Accepted 13 December 2010
Available online 21 December 2010

Keywords:
Soil structure
Image analysis
^{241}Am
Applied nuclear physics
Computed tomography

ABSTRACT

A gamma-ray computed tomography (CT) scanner was used to evaluate changes in the structure of clayey soil samples with surface compaction submitted to wetting and drying (W–D) cycles. The obtained results indicate that W–D cycles promoted an increasing of about 10% in soil porosity with a decreasing of about 6% in soil bulk density of this compacted region. With the use of the CT it was also possible to define the thickness of the compacted region that in our case was of about 8.19 mm. This last information is very important, for instance, to estimate hydraulic parameters in infiltration models. Finally, CT analysis showed that the compacted region remained at the surface samples, even after the application of the W–D cycles.

1. Introduction

Computed tomography (CT) was first introduced into medical science, and lately with the success of the technique, CT began to be used in other areas of knowledge (Cattle, 2007; Peele et al., 2006; Masschaele et al., 2004). In the field of soil science tomography was first used in measurements of soil bulk density and soil water content, and several contributions have been made to this area afterwards (Pedrotti et al., 2005; Braz et al., 2001).

CT using X- and gamma-rays is a non-invasive method that gives a detailed analysis of soil bulk density (ρ_b) and porosity (P) variability along a cross-section of a soil sample. CT images usually employed in soil science are obtained with resolutions of the order of millimeters to micrometers.

CT is based on the computation of the cross-sectional distribution of a physical property of a material from projections taken from a number of different directions. The reconstruction of a CT image is given by the definition of a plane or cut using a coordinate system (x, y) to locate measurement points.

Mathematically, it is possible to define a density function $f(x, y)$, which represents the cross-sectional distribution of the soil physical property of interest. CT has, as the main objective, the reproduction of this function as accurately as possible. In the case of gamma-ray CT, $f(x, y)$ represents the linear attenuation coefficient (μ) of the material under analysis (Kak and Slaney, 1988).

Compaction of the upper soil surface is an important phenomenon that may occur due to the impact of raindrops on bare soils, which promotes the disintegration of soil aggregates and the dispersion of the clay particles in the soil suspension. The thickness of these little compacted regions can vary from 0.1 mm up to values exceeding 50 mm (Valentin and Bresson, 1992). These compacted regions can be influenced by the repetition of wetting and drying (W–D) cycles during measurements of soil physical properties such as the soil water retention curve (SWRC).

The repetition of wetting and drying (W–D) cycles can cause important changes on the structure of a soil as reported in the literature by several authors (Pillai-McGarry and Collis-George, 1990; Bresson and Moran, 2004; Denef et al., 2001). The soil pore system (SPS) that is directly related to the temporal and spatial distribution of soil water content can strongly be affected by the application of W–D cycles due to the irreversible rearrangement of soil particles inside the matrix frame (Sarmah et al., 1996; Pillai and McGarry, 1999; Langmaack et al., 2002). Changes of soil structure due to W–D cycles have important practical consequences when calculating soil water storages and matric potentials, widely used in irrigation management.

So the purpose of this research was twofold: first, to verify the potential of CT to give detailed analysis of soil bulk density and porosity, and second, to analyze the effect of repetitions of W–D cycles in the dynamic of samples with surface compaction during SWRC evaluation. The soil wetting was obtained through the capillary rise method as traditionally made. Changes in the compacted region were evaluated by using gamma-ray CT image analysis with millimetric resolution.

* Corresponding author. Tel.: +55 42 3220 3044; fax: +55 42 3220 3042.
E-mail addresses: lfpires@uepg.br, luizfpires@gmail.com (L.F. Pires).

0969-806X © 2010 Elsevier Ltd. Open access under the Elsevier OA license.
doi:10.1016/j.radphyschem.2010.12.006

2. Material and methods

2.1. Experimental area and sampling

The study area is located in Piracicaba, São Paulo State (SE Brazil – 22°4′S; 47°38′W; 580 m a.s.l.), on a soil characterized as a Dark Red Latosol (LVE) (260 sand, 260 silt, 480 clay, and 20.2 g kg^{-1} organic matter), clayey texture. The average annual rainfall, relative humidity, and air temperature are 1253 mm/year, 74%, and 21.2 °C, respectively. The dry season covers June–August, July being the driest month. During spring-summer, October to March, very high intensity rainfall events are common, several of them reaching intensities of 50 mm/h or more.

Five samples were collected from the surface layer (0–10 cm) with steel cylinders (h=3.0 cm, D=4.8 cm, V=55 cm^3). The sampler was inserted into the soil by impact, with a rubber hammer falling from a fixed height, as traditionally made. After complete insertion of the cylinders into the soil, the surrounding soil was carefully removed to minimize further soil disturbance due to vibration, shear stress, and compaction. The excess of soil at upper and bottom surfaces was carefully trimmed off and made flat to be sure that the soil volume was approximately equal to the internal volume of the cylinder.

2.2. Wetting and drying (W–D) cycles

Soil samples were saturated by the capillary rise method. The wetting (W) procedure consisted in soaking the samples in a tray with the water level just below the top of the steel rings. It was found that twenty-four hours were necessary to saturate the samples and to minimize entrapped air bubbles (Klute, 1986), which can cause slaking of soil aggregates. Thereafter samples were partially dried by submitting them to a 400 kPa pressure in a pressure chamber. After drying samples were again saturated and submitted to a new pressure application, in this way being submitted to a series of W–D cycles. This wetting and drying procedure is exactly the same employed to evaluate water retention curves by the Richards method (Klute, 1986). Three treatments were investigated: 0 W–D, the control treatment, in which samples were not submitted to W–D cycles; 3 W–D, samples submitted to 3 W–D cycles, and 9 W–D, samples submitted to 9 W–D cycles.

2.3. CT scanner

The scanning of core samples was performed with a first generation CT scanner with fixed source–detector arrangement and translation/rotational movements of the samples (Fig. 1). The radioactive source used was ^{241}Am (59.54 keV) with an activity of 3.7 GBq. NaI(Tl) scintillation crystal (7.62 × 7.62 cm) coupled to a photomultiplier tube was used to detect the monoenergetic photons passing through circular lead collimators (1 mm) mounted between source and detector. Samples were rotated over 180° in intervals of 2.25°, with linear movement intervals of 0.10 cm.

The acquired data were stored in a PC and CT images were obtained using the reconstruction algorithm Microvis developed by Embrapa Agricultural Instrumentation Center (CNPDIA) located in São Carlos, SP, Brazil. A matrix with resolution of 80 × 80 was obtained for each scanning. This represents that 6400 tomographic unit (TU) values were obtained for each sample. The measuring time for each count was 26 s, giving a ≈46.5 h total exposure time per tomography experiment, including the time for rotating and translating the sample. The average incident monoenergetic photon flux densities (number of photons m^{-2} s^{-1}) was 10,800.

The calibration of the system was made through the correlation between the linear attenuation coefficients, μ (cm^{-1}), of different homogeneous materials and their respective tomographic unities (TUs) obtained by the image reconstruction program (Pedrotti et al., 2005).

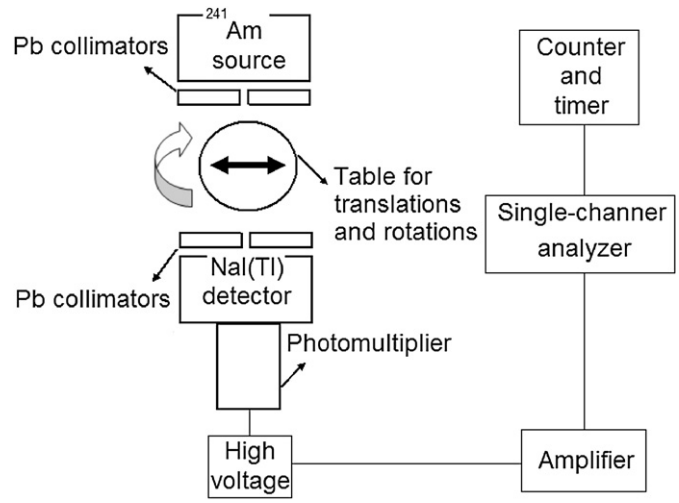

Fig. 1. Schematic diagram of the first generation gamma-ray computed tomography (CT) scanner.

2.4. Image processing and data analysis

For each sample four regions (layers) were selected (0–7 mm (A); 7–14 mm (B); 14–21 mm (C); 21–28 mm (D)) for quantitative image analysis. The first (layer A) was located in the compacted region and the others (layers B–D) below this region. Each layer is represented by six ρ_b or P values (obtained for layers of about 1.2 mm).

CT analyses were performed on the very same soil samples before any W–D cycle and after 3 and 9 W–D. The planes of image acquisition were vertical, in the direction of the central axis of the cylinders and the available data permitted a continuous 2-D analysis of TU distributions and, consequently, of ρ_b and P variations along that cross-section of the sample.

Soil bulk density, ρ_b (g cm^{-3}), evaluated by CT was calculated substituting δ (angular coefficient) of the calibration curve by the mass attenuation coefficients (μ_m) of water and soil (cm^2 g^{-1}), in the Beer–Lambert equation, as derived by Pedrotti et al. (2005):

$$\rho_b = \frac{(TU/\delta) - \mu_{mw}\theta_r\rho_w}{\mu_{ms}} \quad (1)$$

where θ_r (cm^3 cm^{-3}) represents the volumetric soil water content of the air dry sample before CT scanning and ρ_w (g cm^{-3}) is the water density.

The measurement of P was made using

$$P(\%) = \left(1 - \frac{\rho_b}{\rho_p}\right)100 \quad (2)$$

where ρ_p (g cm^{-3}) is the soil particle density. Details about the method used to measure ρ_p can be found in Flint and Flint (2002).

The per cent relative error (RE) between the values of ρ_b for the surface compacted region (Layer A) and for the layers below this region (Layers B–D) was calculated according to:

$$RE(\%) = \left|\frac{\rho_{b(A)} - \rho_{b(B-D)}}{\rho_{b(A)}}\right|100 \quad (3)$$

The soil surface compacted region was defined through the image analysis of 2-D TU maps. These maps were generated by softwares that allow the construction of surface maps of the TU matrix obtained after CT scanning. During the construction of

surface maps TU values were separated in different TU strips. The surface compacted region was defined choosing the strip with the highest TU values.

3. Results and discussion

From the 2-D images, 2-D TU maps, and TU distributions it is possible to observe the structure modification of the soil compacted region (Fig. 2a–i). The control sample (Fig. 2a and d) shows the existence of large compacted regions at the upper surface (Layer A). We can observe an important decrease of this soil compacted region after the application of 9 W–D cycles (Fig. 2c and f). However, there are practically no visual important modifications in the compacted surface region between samples submitted to 0 (Fig. 2a and d) and 3 W–D cycles (Fig. 2b and e).

The mass attenuation coefficients, for the 59.54 keV photons, for the LVE soil and water were 0.307 ± 0.003 and 0.199 ± 0.003 cm^2 g^{-1}, which agree with values found in the literature for ^{241}Am sources (Ferraz and Mansell, 1979). The slope (δ) of the linear regression between μ and TU was 0.959 cm (R=0.99). These results were used to calculate ρ_b and P by the CT method using Eqs. (1) and (2). Averages ρ_p obtained for six replicates of the LVE soil were 2.53 ± 0.03 g cm^{-3}, which agree with values found in the literature for clayey soils (Grohmann, 1960).

Below the morphologically defined compacted region by 2-D tomographic images (about 7 mm thick), it is possible to observe increases in P with depth among treatments (Fig. 3). This result is very evident for the compacted region. The most important differences in P occurred between 0 and 9 W–D. The analysis of P profiles allowed us to obtain a better comprehension of the structure changes showed by soil images (Fig. 2a–c) and to measure porosity values for layers of about 1.2 mm which, as already said, cannot be achieved by traditional techniques of analysis in a non-destructive way.

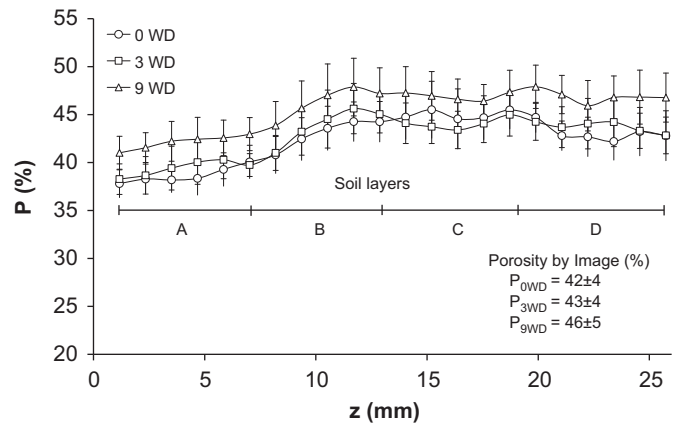

Fig. 3. Porosity (P) by image variations along depth (z) for core samples not submitted to any wetting and drying (W–D) cycles (0 W–D) and submitted to 3 and 9 W–D cycles (3 and 9 W–D). The error bars represent the standard deviation of average P (five replicates).

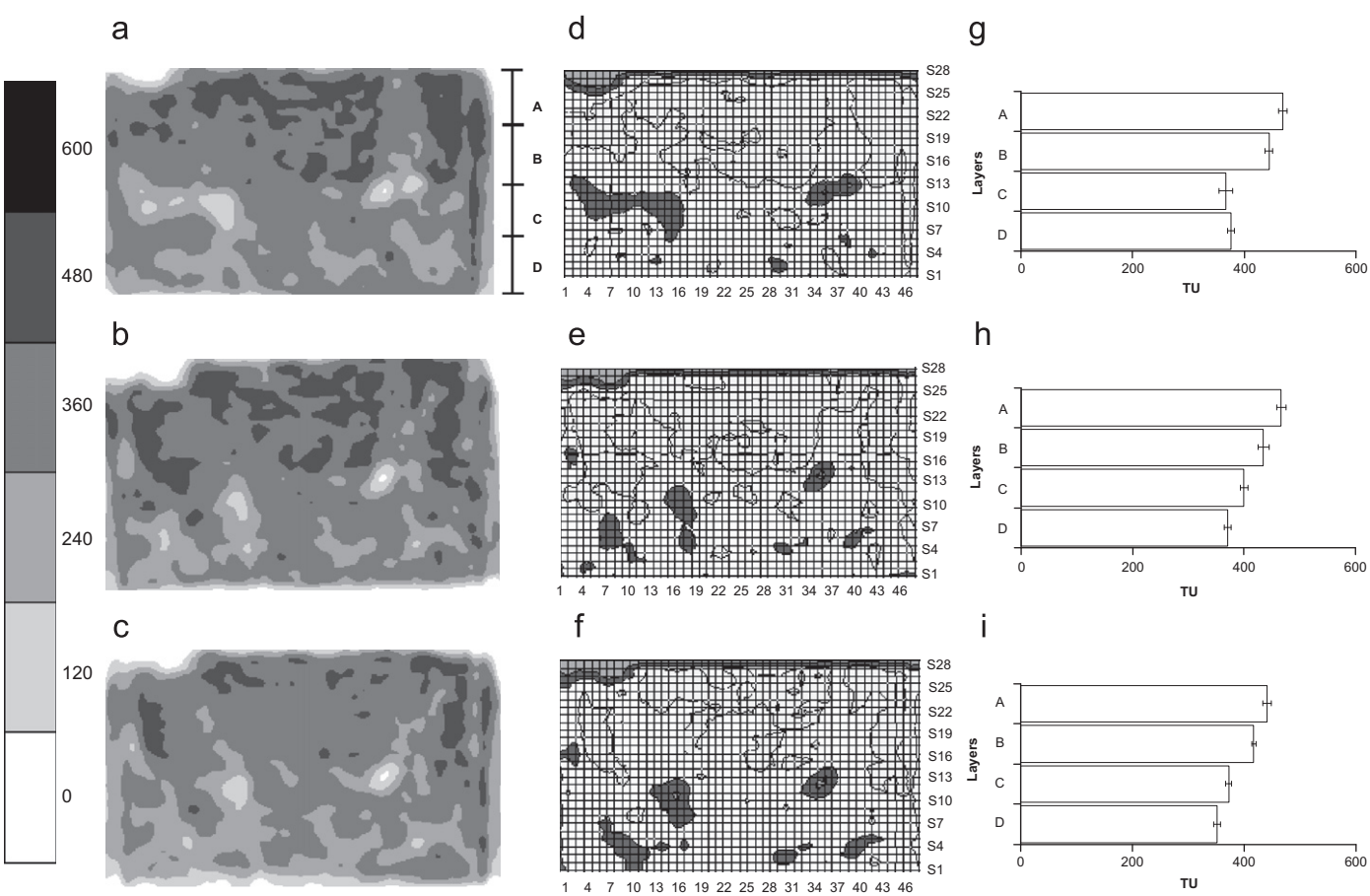

Fig. 2. (a–c) 2-D tomographic images of core samples used to evaluate soil bulk density (ρ_b) and porosity by image (P) variations of compacted surface layers with the application of wetting and drying (W–D) cycles. Scale indicates tomographic unit (TU) values. (d–f) 2-D TU maps of tomographic images (matrix of 1269 (47 × 27) TU values). (g–i) TU distributions along depth. 0 W–D (a–d–g); 3 W–D cycles (b–e–h), and 9 W–D cycles (c–f–i). Letters A–D represent soil layers (each layer represents average of six TU values). The error bars represent the standard deviation of average TU (six values).

A possible explanation for the increases in P with the applications of W–D cycles can be explained by macropore development (Fig. 4a and b) due to the friction between the soil sample and the cylinder wall during wetting and subsequent drying. The internal stress between the soil and the cylinder surface can cause a small increase in the soil volume during wetting, but after drying this volume cannot return to its original value. This effect may become worse after sequences of W–D cycles causing the appearance of small cracks or holes inside the soil structure.

W–D cycles affect the soil pore system due to internal stresses, which changes irreversibly the soil structure after sequences of wetting and drying (Baumgartl, 1998). Bresson and Moran (2004) have demonstrated that soil samples when submitted to wetting by capillary rise can present microcrackings of many aggregates with an irregular pattern and wide spacing producing important structural changes. Dexter (1988) observed that W–D cycles directly affect the soil aggregation due to the action of forces among soil particles and between aggregates. Consequently, the soil porous system will strongly be influenced by the sequences of W–D. These sequences result in small changes in the soil core sample volume,

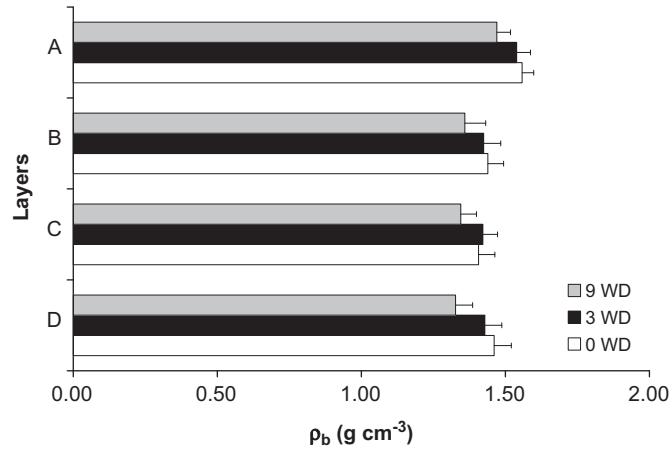

Fig. 5. Changes in soil bulk density (ρ_b) with repetitions of wetting and drying (W–D) cycles along soil layers (0–7 mm (A); 7–14 mm (B); 14–21 mm (C); 21–28 mm (D)) inside CT images. The error bars represent the standard deviation of average ρ_b (five replicates).

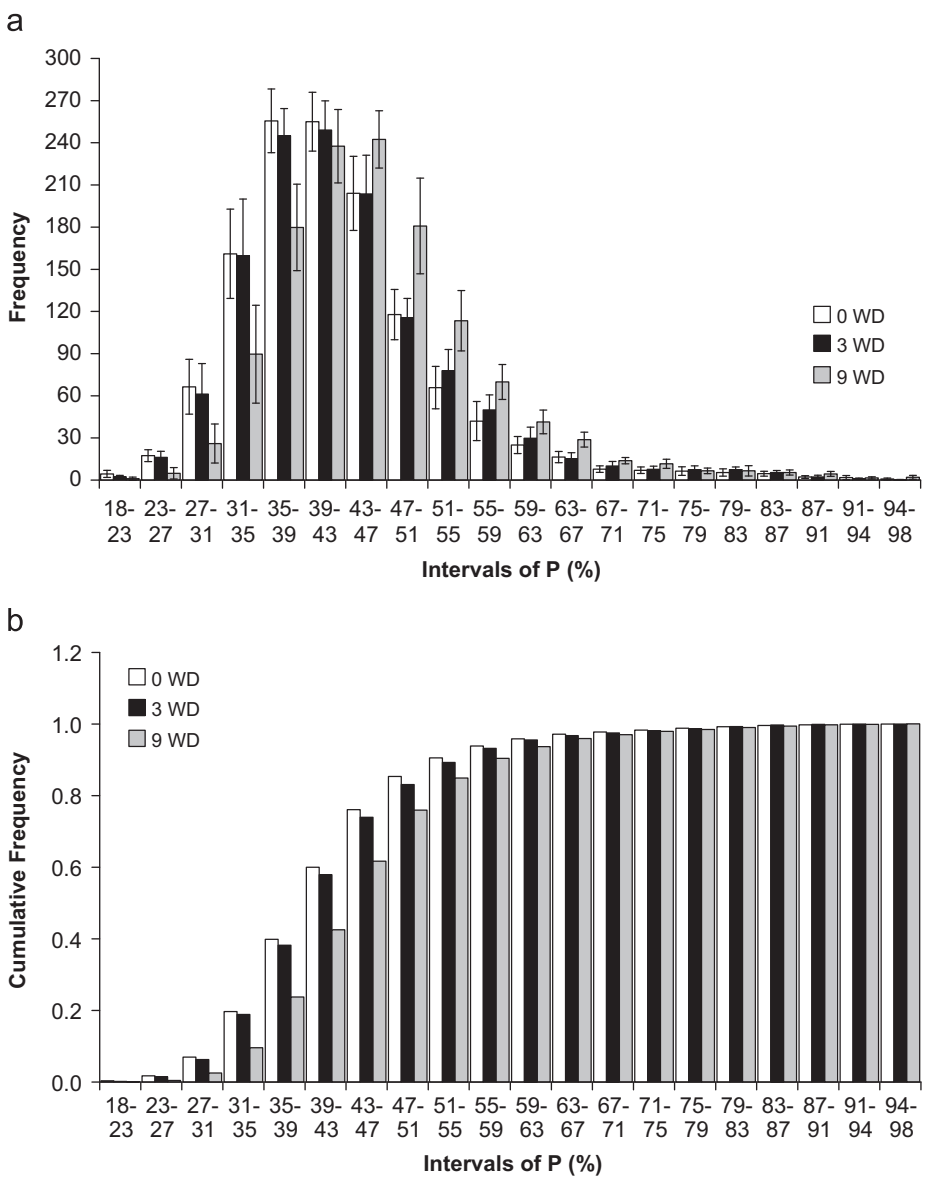

Fig. 4. (a–b) Changes in porosity (P) by image evaluated for different intervals of P. 0 W–D represents samples not submitted to any wetting and drying (W–D) cycles, and 3 and 9 W–D samples submitted to 3 and 9 W–D cycles, respectively. The error bars represent the standard deviation of average P (five replicates).

caused by stresses due to water/air interfaces originated from capillary forces. Therefore, after each new wetting the soil structure will undergo alterations to a new state of energy, which most of the time promotes definitive changes in soil structure like the formation of connected soil pores (Viana et al., 2004).

Fig. 5 indicates the variations of average ρ_b values for the different soil layers shown in Fig. 2. All the five samples of the LVE soil demonstrated marked compacted regions at the surface. However, after the procedure of wetting and drying used in this work all samples had decreases in ρ_b at this compacted region (Layer A) showing that these cycles can cause important changes in the soil structure of samples with surface compaction.

A comparison of mean P variations for the compacted surface (Layer A) and layers below this region (Layers B–D) with applications of W–D cycles is given in Table 1. Relative differences at the compacted region between 0 and 9 W–D where 7.7% and for layers below this region were 6.8%. Per cent relative error (RE) analyses between P values calculated at the surface compacted region (Layer A) and at the other layers (Eq. (3)) demonstrate practically constant REs among treatments. Through these results we can conclude that even after 9 W–D cycles the LVE soil still shows the existence of a residual compacted layer at the upper surface.

Table 1
Porosity (P) by image variations due to application of wetting and drying (W–D) cycles.

Treatments	P (%)		
	Control	3 WD	9 WD
Compacted layer	39 ± 2	39 ± 2	42 ± 2
Layers B–D	44 ± 4	44 ± 4	47 ± 5
RE (%)	12.8	12.8	11.9

Standard deviations represent the scatter of five porosity values for each treatment; RE is the per cent relative error; control is related to samples not submitted to W–D cycles (0 WD); 3 WD, samples submitted to 3 consecutive W–D cycles, and 9 WD, samples submitted to 9 consecutive W–D cycles.

In our study, the decrease in ρ_b with depth is non-linear (Fig. 6). Fox et al. (2004) reported similar results when working with a sandy loam soil. The greatest mean ρ_b values at the compacted surface layer (Layer A) in comparison to the other layers confirm the presence of a compacted region at the soil surface.

The best mathematical adjustment of ρ_b for the LVE was obtained by using a first decay exponential function (Fig. 6). The greatest change in ρ_b occurred in the top 10 mm and beyond this depth the change in this soil physical property appears to be negligible. Through the mathematical fit it is possible to conclude that the application of W–D cycles can influence the region of compaction and more homogeneous layers can be found after the first layer (Layer A). However, the application of 9 W–D cycles (Fig. 6c) is not sufficient to decrease the soil density gradient along depth (soil layers). After 9 W–D the difference between ρ_0 and ρ_b (at 0 mm) obtained by the mathematical adjustment is 0.22 g cm^{-3}, while for the control sample (0 W–D) is 0.24 g cm^{-3}. Bresson et al. (2004) and Fohrer et al. (1999) also observed similar results by using a medical X-ray CT. The last authors observed a maximum ρ_b 1 mm below the soil surface and its value also decreased exponentially with depth up to 10 mm when it merged with the initial ρ_b.

The mathematical adjustments of the soil bulk density profile with depth allow us to define a transition zone for the sample with surface compaction (Fox et al., 2004). Layer B appears to be a transition zone for the LVE soil below the compacted region (Layer A). This type of information is very important because changes in ρ_b with depth can

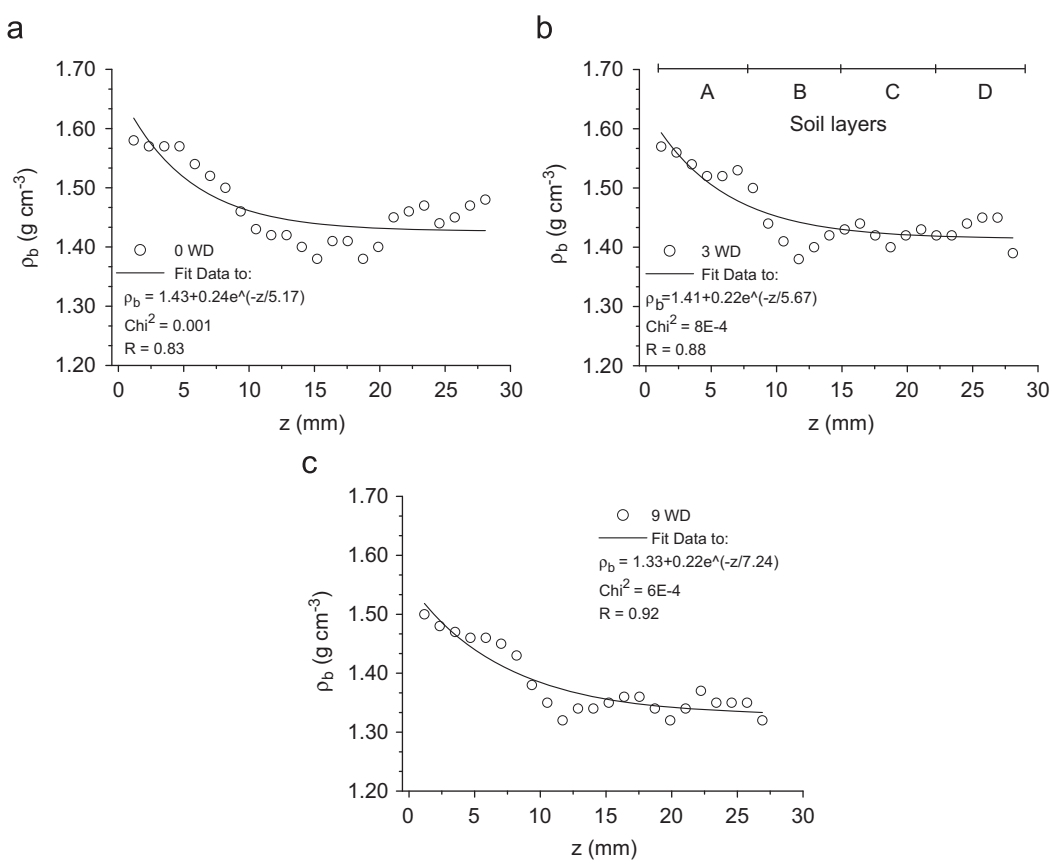

Fig. 6. Variations in the soil bulk density (ρ_b) with depth (z) for each analyzed layer (0–7 mm (A); 7–14 mm (B); 14–21 mm (C); 21–28 mm (D)) for the Dark Red Latosol for: (a) core samples not submitted to any wetting and drying (W–D) cycles (0 W–D), (b) cores samples submitted to 3 W–D cycles, and (c) core samples submitted to 9 W–D cycles.

be helpful for the estimation of hydraulic parameters in infiltration models.

To conclude, the results obtained in this work (Figs. 2–6) confirm that wetting and drying cycles – by the capillary rise method – can cause important modifications in the soil porous system of samples with surface compaction. Through CT analysis it was possible to analyze changes in soil structure of a very same sample, which cannot be obtained by using traditional techniques of image analysis. The procedure of sample saturation by the capillary rise method is frequently used during SWRC evaluations (Klute, 1986). Therefore, alterations in soil porosity distribution (Fig. 4) due to repetitions of W–D cycles will directly affect the representativeness of SWRCs, which are used for estimations of water retention and movement, widely used in irrigation management.

Acknowledgement

The authors are grateful to Conselho Nacional de Desenvolvimento Científico e Tecnológico (CNPq) for the financial support and PQ grantings.

References

Baumgartl, Th., 1998. Physical soil properties in specific fields of application especially in anthropogenic soils. Soil Till. Res. 47, 51–59.

Braz, D., Barroso, R.C., Lopes, R.T., Anjos, M.J., de Jesus, E.F.O., 2001. Evaluation of scatter-to-primary ratio in soil CT-imaging. Radiat. Phys. Chem. 61, 747–751.

Bresson, L.M., Moran, C.J., 2004. Micromorphological study of slumping in a hardsetting seedbed under various wetting conditions. Geoderma 118, 277–288.

Bresson, L.M., Moran, C.J., Assouline, S., 2004. Use of bulk density profiles from X-ray radiography to examine structural crust models. Soil Sci. Soc. Am. J. 68, 1169–1176.

Cattle, B.A., 2007. A model problem for restricted-data gamma ray emission tomography of highly active nuclear waste. Ann. Nucl. Energy 34, 591–599.

Denef, K., Six, J., Paustian, K., Merckx, R., 2001. Importance of macroaggregate dynamics in controlling soil carbon stabilization: short-term effects of physical disturbance induced by dry–wet cycles. Soil Biol. Biochem. 33, 2145–2153.

Dexter, A.R., 1988. Advances in characterization of soil structure. Soil Till. Res. 11, 199–238.

Ferraz, E.S.B., Mansell, R.S., 1979. Determining water content and bulk density of soil by gamma ray attenuation methods. Technical Bulletin 807, 51 IFAS (Institute of Food and Agricultural Sciences, Unversity of Florida).

Flint, A.L., Flint, L.E., 2002. The solid phase: particle density. In: DANE, J.H., TOPP, G.C. (Eds.), Methods of Soil Analysis. Part 4. Physical Methods. ASA, Madison; SSSA, pp. 229–240.

Fohrer, N., Berkenhagen, J., Martin Hecker, J., Rudolph, A., 1999. Changing soil and surface conditions during rainfall single rainstorm/subsequent rainstorm. Catena 37, 355–375.

Fox, D.M., Bryan, R.B., Fox, C.A., 2004. Changes in pore characteristics with depth for structural crusts. Geoderma 120, 109–120.

Grohmann, F., 1960. Distribuição do tamanho de poros em três tipos de solos do Estado de São Paulo. Bragantia 19, 319–328.

Kak, A.C., Slaney, M., 1988. Principles of Computerized Tomographic Imaging. IEEE Press, New York, USA 327 pp.

Klute, A., 1986. Water retention: laboratory methods. In: Black, C.A. (Ed.), Methods of Soil Analysis. I. Physical and Mineralogical Methods. ASA, Madison; SSSA, pp. 635–662.

Langmaack, M., Schrader, S., Rapp-Bernhardt, U., Kotze, K., 2002. Soil structure rehabilitation of arable soil degraded by compaction. Geoderma 105, 141–152.

Masschaele, B., Dierick, M., Cnudde, V., van Hoorebeke, L., Delputte, S., Gildemeister, R., Gaehler, R., Hillenbach, A., 2004. High-speed thermal neutron tomography for the visualization of water repellents, consolidants and water uptake in sand and lime stones. Radiat. Phys. Chem. 71, 807–808.

Peele, A.G., Quiney, H.M., Dhal, B.B., Mancuso, A.P., Arhatari, B., Nugent, K.A., 2006. New oppotunities in X-ray tomography. Radiat. Phys. Chem. 75, 2067–2071.

Pedrotti, A., Pauletto, E.A., Crestana, S., Holanda, F.C.R., Cruvinel, P.E., Vaz, C.M.P., 2005. Evaluation of bulk density of Albaqualf soil under different tillage systems using the volumetric ring and computerized tomography methods. Soil Till. Res. 80, 115–123.

Pillai, U.P., McGarry, D., 1999. Structure repair of a compacted Vertisol with wet–dry cycles and crops. Soil Sci. Soc. Am. J. 63, 201–210.

Pillai-McGarry, U.U.P., Collis-George, N., 1990. Laboratory simulation of the surface morphology of self-mulching and non self-mulching Vertisols. I. Materials, methods and preliminary results. Aust. J. Soil Res. 28, 129–139.

Sarmah, A.K., Pillai-McGarry, U., McGarry, D., 1996. Repair of the structure of a compacted Vertisol via wet/dry cycles. Soil Till. Res. 38, 17–33.

Valentin, C., Bresson, L.M., 1992. Morphology, genesis and classification of surface crusts in loamy and sandy soils. Geoderma 55, 225–245.

Viana, J.H.M., Fernandes Filho, E.I., Schaefer, C.E.G.R., 2004. Efeitos de ciclos de umedecimento e secagem na reorganização da estrutura microgranular de latossolos. R. Bras. Ci. Solo 28, 11–19.